chemosensors

MDPI

Article

Gas Sensor Based on ZnO Nanostructured Film for the Detection of Ethanol Vapor

Mikayel Aleksanyan, Artak Sayunts *, Gevorg Shahkhatuni, Zarine Simonyan, Gohar Shahnazaryan and Vladimir Aroutiounian

Center of Semiconductor Devices and Nanotechnologies, Yerevan State University, Yerevan 0025, Armenia; maleksanyan@ysu.am (M.A.); gevshahkhatuni@ysu.am (G.S.); z.simonyan@ysu.am (Z.S.); sgohar@ysu.am (G.S.); kisahar@ysu.am (V.A.)

* Correspondence: sayuntsartak@ysu.am; Tel.: +374-60-710319

Abstract: In this paper, the ZnO<La> target was synthesized by the solid-state reaction method and a nanostructured thin film was deposited by the RF (radio frequency) magnetron sputtering method on a Multi-Sensor-Platform. The obtained ZnO<La> nanostructured film was investigated as the sensing material. Energy-Dispersive X-ray (EDX) analysis indicated the existence of La in the synthesized ZnO<La> material. Scanning Electron Microscope (SEM) images of the film showed the grain sizes in the range of 20–40 nm. Sensor performance characteristics such as a dynamic response, response and recovery times, and ethanol detection range were investigated at 50–300 °C. A sensitivity was observed at extremely low concentrations of ethanol (0.7 ppm). The minimum response and recovery times of the sensor corresponding to 675 ppm ethanol vapor concentration at 250 °C were found to be 14 s and 61 s, respectively. The sensor showed a high response, good selectivity, fast response/recovery behavior, excellent repeatability toward ethanol vapor, and low sensitivity toward humidity. These characteristics enable the use of a ZnO<La> based sensor for ethanol detecting applications.

Keywords: ethanol sensor; magnetron sputtering; nanograins; sensitivity; thin film; zinc oxide

Citation: Aleksanyan, M.; Sayunts, A.; Shahkhatuni, G.; Simonyan, Z.; Shahnazaryan, G.; Aroutiounian, V. Gas Sensor Based on ZnO Nanostructured Film for the Detection of Ethanol Vapor. *Chemosensors* **2022**, *10*, 245. https://doi.org/10.3390/chemosensors10070245

Academic Editor: Andrea Ponzoni

Received: 16 May 2022
Accepted: 22 June 2022
Published: 28 June 2022

1. Introduction

Today, the detection of ethanol vapors (C_2H_5OH) and the accurate measurement of their low concentrations are the focus of researchers, as ethanol is considered the most widely used organic compound in areas such as fuel processing, agronomic, biomedical, food, pharmaceutical, hygienic, cosmetic, and chemical industries. In particular, it is known that the composition of chemical compounds emitted from food can be used to analyze its quality and freshness. Among the chemicals emitted from the food, ethanol is considered the most important substance and the detection of its concentration is widely used in modern electronic noses to continuously monitor the quality and freshness of stored groceries and meat. Besides, ethanol is known as a rather toxic and hazardous gas, which can greatly affect human health. It stands out some harmful effects such as vomiting, nausea, skin irritations, low blood pressure, low blood sugar level, etc. Excessive use of alcoholic beverages also leads to drunk driving accidents. Therefore, the rapid detection of ethanol is inevitably required and the ethanol gas sensing materials have been developed [1–6].

Choosing the right material with advanced physical and chemical properties for the design and production of nanoscale devices is one of the most important issues. As one of the most widely used and studied materials, it is essential to develop the ZnO-based nanostructured material as the building blocks for future nanoscale devices. ZnO crystals stand out for their excellent thermal, piezoelectric, optical, electrical as well as semiconductor properties such as a high isoelectric point, tunable resistance, controllable charge-transfer

properties, low impact on the environment, and biocompatibility. Morphologically diverse ZnO thin films consist of nanoparticles that can be easily synthesized using a variety of different methods including Chemical Vapor Deposition (CVD) and Physical Vapor Deposition (PVD) technologies. As one of the well-known CVD technologies, high-frequency magnetron sputtering is considered a very efficient and cost-effective technique for the production of gas sensors [7–10].

Due to its high chemical and thermodynamic stability, catalytic activity, and large surface area to volume ratio, the ZnO polycrystalline material has become one of the main materials used in gas sensors. Among the mainly used metal oxides, ZnO is characterized by its affordability, wide bandgap energy (3.4 eV), easy preparation of nanostructures, large exciton binding energy (60 meV) at room temperature, and high charge-carrier mobility. ZnO is a non-poisonous material in its natural state, which makes it environmentally friendly. Zinc oxide with three different crystal structures (wurtzite, zinc blende, and rock salt) is considered to be one of the most widely used and studied MOS materials due to its distinctive surface properties. Under ambient conditions, the wurtzite structure of ZnO is considered the most thermodynamically and chemically stable phase. Although the polycrystalline structure of this material has quite promising parameters in terms of use in gas sensors, pure ZnO has not represented high sensing performance. Introducing various dopants in this material results in high sensitivity, selectivity, and stability toward both oxidizing and reducing gases [10–13].

In recent years, many papers have been reported related to various metal oxides-based ethanol sensors. Nie et al., synthesized NiO microspheres by a one-step hydrothermal method [14]. The sensor showed a sufficient sensitivity (30) to a rather high concentration of ethanol (400 ppm) at a fairly high operating temperature (350 °C). Tharsika et al. synthesized a mixed structure of ZnO nanorod on SnO_2 thin film using the spray pyrolysis method [15]. Although the sensor response reached a value of 285 toward 100 ppm ethanol vapor, the operating temperature of the sensor was quite high (400 °C), and the detection range started at 20 ppm. Recently, a ZnO-ZnS nanofiber heterostructure-based ethanol sensor has been fabricated by the orthogonal experiment and hydrothermal method [16]. The sensor showed a response of 55.34 to 100 ppm ethanol vapor at 260 °C with a detection range of 20–100 ppm having not so simple manufacturing technology. A low temperature (29 °C) ethanol sensor based on vertically aligned ZnO nanorods decorated with CuO nanoparticles was manufactured by low-temperature solution processing [17]. The sensor with an enhanced gas sensing performance had no good linearity of responses with ethanol vapor concentrations. Organic semiconductors sensitive to ethanol vapor have been also used as a sensitive material in sensor manufacturing technologies [18,19]. In particular, an ethanol sensor based on an organic-field effect transistor was fabricated [20]. The sensor was found to be sensitive to ethanol vapor, and the gas sensitivity mechanism was detailed. Wei et al. synthesized an ethanol sensing material based on the mixture of Polyvinylpyrrolidone (PNVP), Carbon Black (CB) and solvent ethylene glycol (EG) [21]. The low detection limit of the sensor was 40 ppm corresponding to a 1.6% response. As an alternative to the available ethanol sensors, we present an ethanol sensor with the optimal combination of almost all the performance parameters. Thus, the sensor has a relatively low operating temperature, a fairly low detection limit, fast response/recovery behavior, high selectivity, repeatability, linearity, low sensitivity toward humidity as well as a cheap and simple manufacturing technology.

In this study, we have demonstrated a ZnO<La> nanostructured ethanol vapor sensor. For this purpose, the ZnO<La> target was synthesized by the solid-state reaction method and the nanostructured thin film was obtained by the RF magnetron sputtering method. The composition and crystalline characteristics of the material were observed by EDX analysis and scanning electron microscopy, respectively. Thus, the gas sensing behavior of the manufactured sensor was investigated at different temperatures and is discussed in the following parts.

2. Experimental Details

2.1. Synthesis of ZnO<La> Material

The sensor manufacturing process started with purchasing materials. To obtain the ZnO<La> sputtering target, ZnO (99.9%) and La_2O_3 (99.9%) nanopowders were collected from Alfa Aesar (Figure 1a). A ZnO:La_2O_3 ceramic target was prepared by the solid-state reaction method as a magnetron sputtering target. Firstly, the required quantities of the corresponding metal oxide powders (ZnO + 1 at.% La_2O_3) were weighed and well mixed for 10 h. Then, the mixture was heat-treated at 900 °C for 8 h, whereas the initial heat treatment of mixed powders removed the wetness of the metal oxide raw materials, which led to better mixing and grinding of powders. After mixing for 25 h, when the mixture was completely homogeneous, it was pressed (with 2000 N/cm^{-2} pressure) into a cylindrical tablet with a diameter of 60 mm. The pressed ZnO:La_2O_3 based tablet was kept in the programmable furnace Nabertherm, HT O4/16 (with the controller of C 42) in the temperature range of 900–1450 °C for 25 h. In the final stage, after mechanical treatment for removing surface defects, a 2 mm thick cylindrical target with a diameter of 50 mm was obtained for magnetron sputtering (Figure 1b).

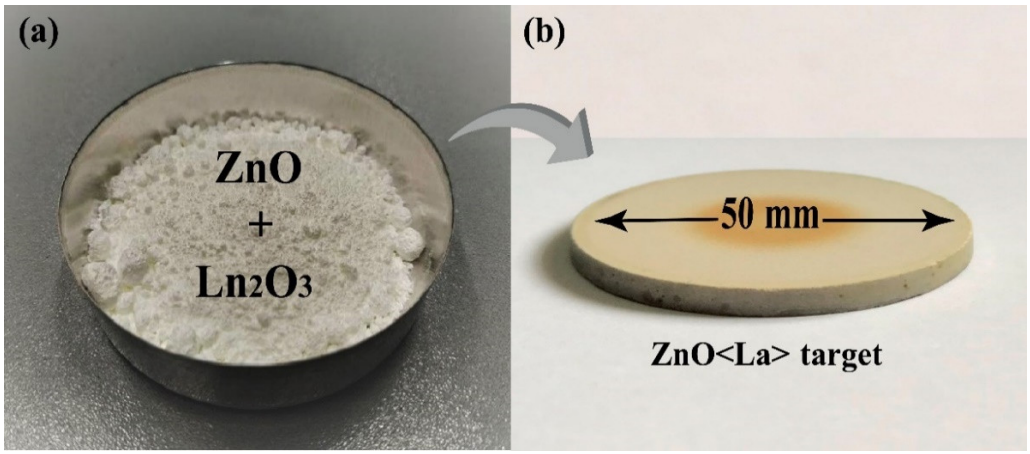

Figure 1. (**a**) Actual photographs of metal oxide powders and (**b**) ZnO<La> sputtering target.

2.2. Gas Sensor Fabrication

The gas sensing layer was deposited on the Multi-Sensor-Platform by the RF magnetron sputtering method using synthesized ZnO<La> target by the VTC-600-2HD DC/RF Dual-Head High Vacuum Magnetron Plasma System (Figure 2). The Multi-Sensor-Platforms were acquired from Tesla Blatna (Blatná, Czech Republic). The sensor substrate was designed for heating, temperature measurement, and resistance recording. Using heat resistance, the chip can be kept at a constant temperature, or a temperature cycle can be operated. The sensor platform consists of a temperature sensor (Pt 1000), a heater, and interdigitated electrode structures (IDES) in a platinum thin film on a ceramic substrate. The platinum heater and temperature sensor were covered with a passive glass layer (Figure 3). The gas sensitive ZnO<La> layer was deposited onto the non-passivated electrode structure, so the Multi-Sensor-Platform was converted into a gas sensor. The fabrication steps of the sensor are presented in Figure 4.

The magnetron sputtering process was carried out under the following technological regimes: 60 W input power, 200 °C deposition temperatures, 70 mm distance between the target and substrate, 2×10^{-3} Pa base pressure, 6×10^{-1} Pa deposition pressure, and 20 min duration of sputtering. Then, the ZnO<La> based sensor was sensitized by the deposition of palladium (99.9%) catalytic particles on the surface of the sensing layer using the ion-beam sputtering method (the cathode current and the anode voltage were equal to 65 A and 25 V, respectively). In the final stage of the sensor production, it was annealed for 4 h at 300 °C for the stabilization of gas sensing parameters and the improvement of the long-term stability.

Figure 2. Actual photograph of the VTC-600-2HD DC/RF Dual-Head High Vacuum Magnetron Plasma System.

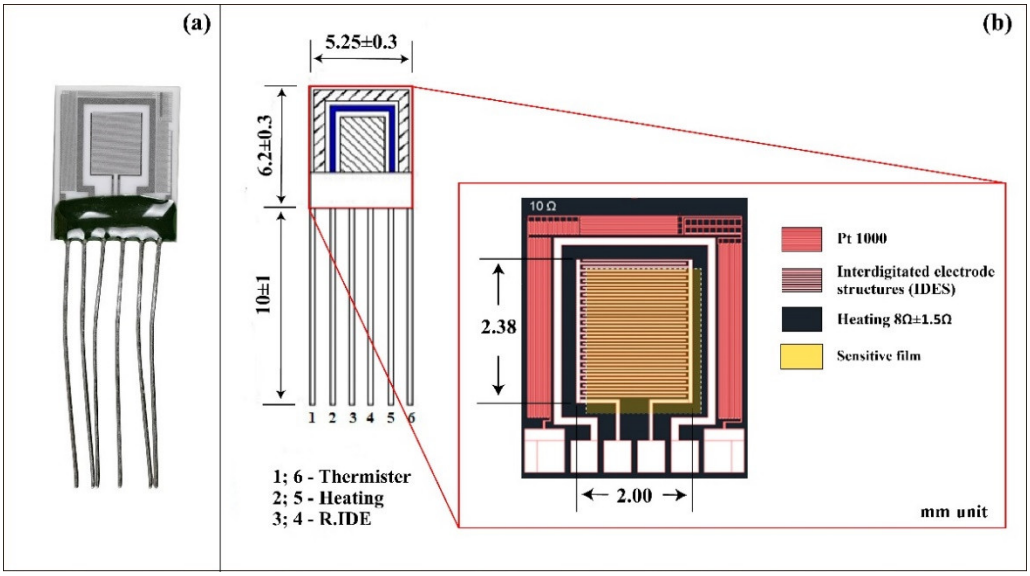

Figure 3. (**a**) Actual photo and (**b**) schematic illustration of the gas sensor.

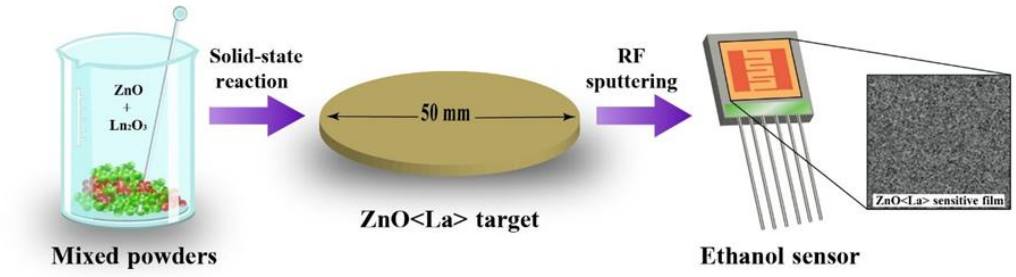

Figure 4. Schematic block diagram of the ethanol sensor fabrication.

2.3. Gas Sensing Test

Using the laboratory-designed (computer-controlled) gas testing system [22], the gas sensing behavior of the ZnO<La> sensor were studied in the air and in the presence of ethanol vapors. To get a required concentration of C_2H_5OH in the 2 L chamber, the aqueous solution of ethanol was injected into the measuring chamber on a specially designed heated container for the rapid conversion of the ethanol in the liquid phase to the gas phase. The real concentrations in ppm unit of ethanol, acetone, water, toluene, dimethylformamide (DMF), and ammonia vapors were determined by the method described in [23]. During the measurement of the resistance change of the sensing layer 5 V DC voltage bias was applied across the sample. For the heating of the active surface of the sensor in the range of 25–300 °C, voltage biases in the range of 0–5 V were applied to the platinum heater. As a quantitative characteristic of the sensitivity, the response of the fabricated sensor is defined, as the resistance ratio of the sensitive film ($R = R_{air}/R_{gas}$), measured in air (R_{air}) and in the presence of ethanol gas (R_{gas}).

2.4. Characterization

The thickness of the interdigitated electrode of the Multi-Sensor-Platform was measured by the Alpha-Step D-300 (KLA Tencor, Milpitas, CA, USA) profiler. The measured result of the electrode-substrate transition profiles is shown in Figure 5a. The thickness of the electrodes varies in the range of 800–900 nm, and the width of the gaps between the electrodes is about 15 microns.

It is known that the performance of resistive sensors is greatly influenced by the thickness value of the sensing film. The optimal thickness of the sensitive film can be decisive in the fabrication of a gas sensor with enhanced parameters. Sensors based on the thick film (>300 nm) sometimes show insufficient speed and sensitivity due to their high ratio of the film thickness and the electron depletion layer (they have an unaffected bulk area), while sensors with extremely thin films (<40 nm) demonstrate the instability of parameters over time. This is mainly due to the creation of crystalline cracks in a thin layer over time and the formation of agglomerations of nanoparticles. The choice of the optimal value of the thickness is decisive for improving the performance parameters of the sensor [24–28]. The thickness of the obtained ZnO<La> thin film was also measured by the Alpha-Step D-300 (KLA Tencor) profiler and it was equal to 72 nm corresponding to 60 W input power and 20 min duration of sputtering process (Figure 5b).

SEM images were obtained using secondary and back-scattered electron signals (SE and BSE, respectively) through a VEGA TS 5130MM (with microanalysis system of INCA Energy 300) instrument (Figure 6a,b). The weight and atomic percent of different elements in the given ZnO<La> material were determined by EDX analysis and shown in Figure 6c. It is confirmed that La is almost homogeneously dispersed in the synthesized ZnO material expressed in the form of white dots (Figure 6b,d). The presence of Zn, La, and O peaks are clearly visible in the quantitative analysis of the EDX spectrum, which indicates the existence of La in the synthesized ZnO<La> material. The actual concentration of La (0.84 at.%) in the ZnO<La> target material is slightly different from the initial calculated concentration (1 at.%), which is assumed due to the certain losses of the material during the mixing and milling of the powders and the error of the measuring instruments.

The morphological structure of the deposited ZnO<La> film was analyzed by scanning electron microscopy using the VEGA TS 5130MM instrument (Figure 7a,b). It is obvious that the film has a granular structure with high homogeneity. Gas sensing parameters are largely determined by the sizes of the grains in the sensitive film, while their dimensions can be actually controlled by changing the power of the magnetron generator. Typically, at a higher power of the generator, argon ions strike the target with higher kinetic energy, which results in a larger size of grains released from the target. At a lower power of the generator, the kinetic energy of the bombarding ions decreases, and consequently, the size of the particles released from the target decreases, while excessive reduction of the power can stop the deposition process. Therefore, it is obvious from the SEM images that the

average grain sizes in the film are in the range of 20–40 nm corresponding to the power of 60 W.

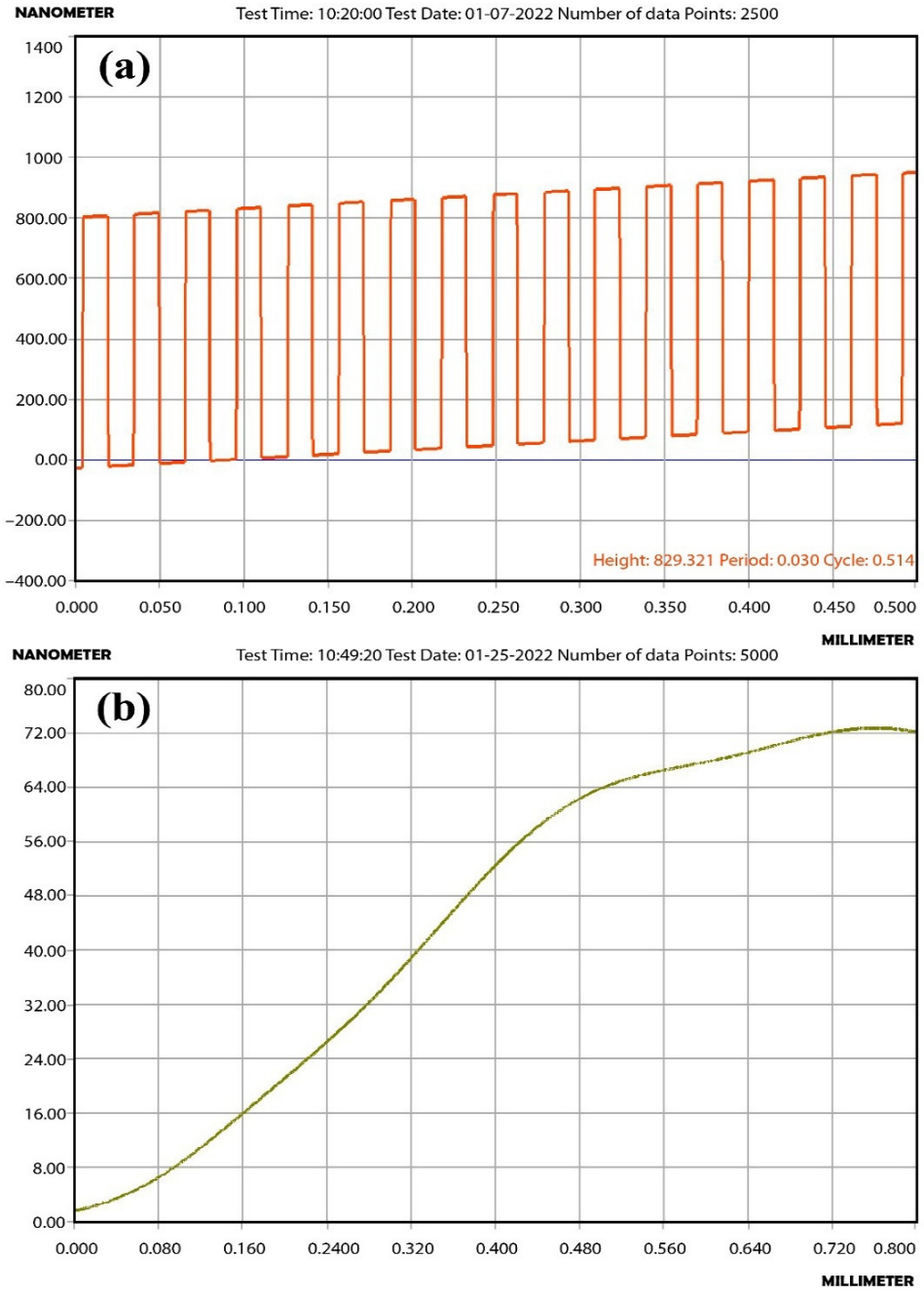

Figure 5. (**a**) The thickness measurement results of the interdigitated electrodes and (**b**) the ZnO<La> film.

The EDX elementary analysis of the sputtered ZnO<La> based thin film is also well examined by the VEGA TS 5130MM instrument (Figure 7c,d). Figure 7d shows that there are clearly depicted peaks of Zn, Al, La, and O, where the presence of Al is conditioned by the Al_2O_3-based substrate. In order to separate the values of the concentrations of the elements contained in the film from the elements of the substrate, the obtained results were processed by the StrataJem program. The actual concentration of La in the ZnO<La> based film is 0.81 at.%, which is not significantly different from its concentration in the ZnO<La> based target material (0.84 at.%).

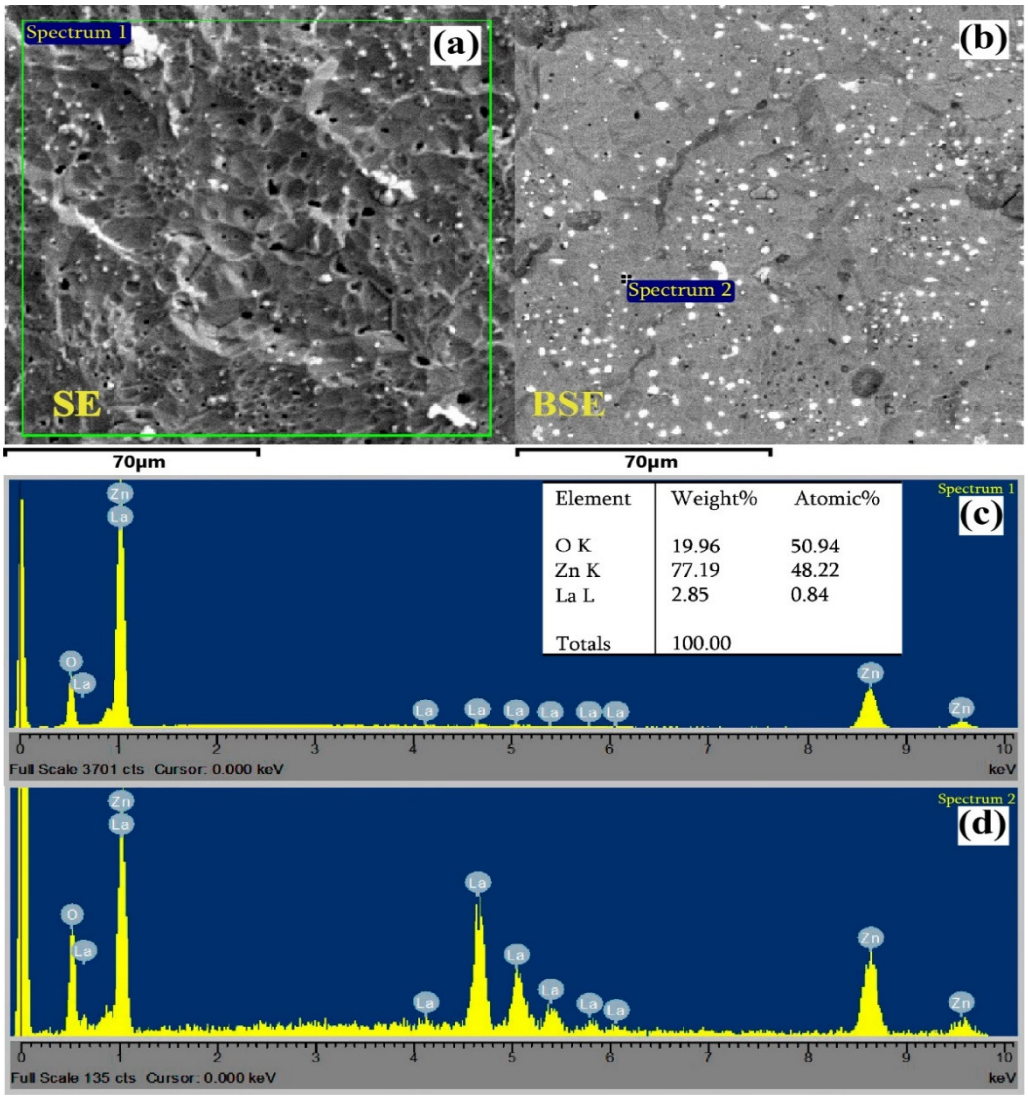

Figure 6. (**a**) SEM SE, (**b**) BSE plane-view and (**c**,**d**) EDX spectrum of the ZnO<La> material.

Elemental mapping analysis of the ZnO<La> film was carried out by EDX spectroscopy. The SEM image, the corresponding results of elemental mapping analysis of the ZnO<La> film, and the X-ray intensity of characteristic lines of different elements are presented in Figure 8. It is obvious that the distribution of elements Zn, Al, O, and La is even, differed from each other by colors in the mapping.

The ZnO<La> film was analyzed by FTIR spectra by NEXUS FT-IR (Nicolet) on two different substrates with different optical transmission ranges (Substrate 1: 1100–230 cm^{-1} and Substrate 2: 4000–2300 cm^{-1}). The strong intensity peak at around 400 cm^{-1} shows the presence of Zn–O [29] and the almost imperceptible peak in the wavenumber range of 500–600 cm^{-1} is supposed to be attributed to lanthanum [30], which is due to its very low concentration in ZnO material (Figure 9a). FTIR study was also carried out in the range of higher wavenumbers (4000–2300 cm^{-1}) to detect hydroxide groups on the film surface. The peaks corresponding to the pronounced hydroxide states (O-H) are mainly in the range of 3200–3600 cm^{-1} [31]. As shown in Figure 9b, there are no strong intensity peaks in the indicated range, which confirms the absence or insignificant amount of hydroxide groups in the film.

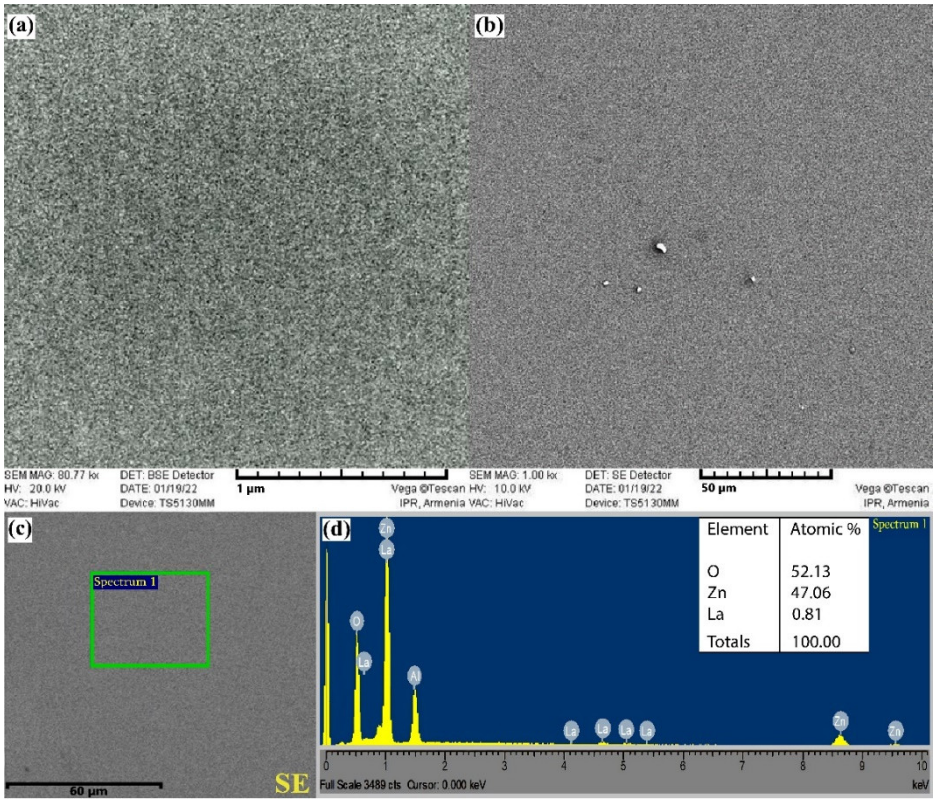

Figure 7. (**a**,**b**) SEM images, (**c**) SEM SE plane-view and (**d**) EDX spectrum of the ZnO<La> film.

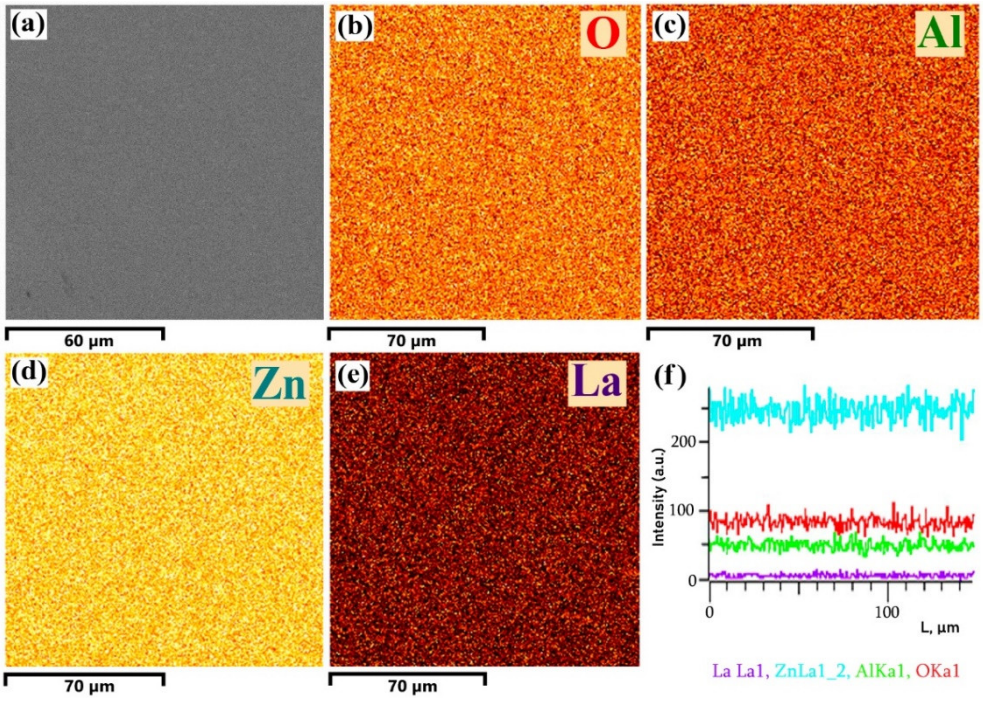

Figure 8. (**a**) SEM image, (**b**–**e**) EDX elemental mapping analysis of Zn, Al, O, and La, and (**f**) X-ray intensity of characteristic lines of different elements.

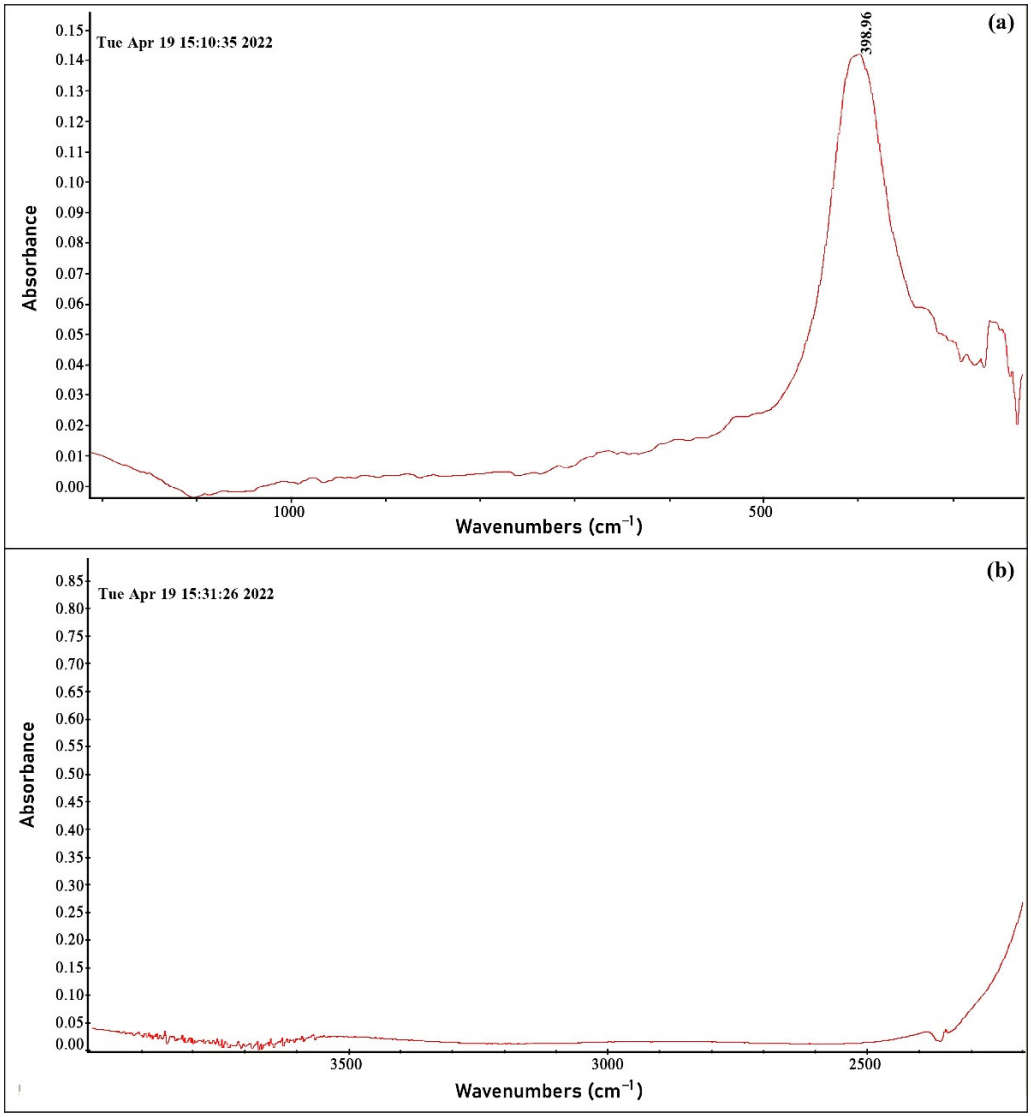

Figure 9. FTIR spectrum of the ZnO<La> film in the wavenumber range of (**a**) 1100–230 cm^{-1} and (**b**) 4000–2300 cm^{-1}.

3. Results and Discussion

3.1. Gas Sensing Studies

To study the gas sensing properties and to select the optimal operating temperature of the ZnO<La> sensor, the dependence of the sensor resistance on the temperature in the air was removed (Figure 10a), and the response values of the sensor were measured in the temperature range of 50–300 °C toward 675 ppm of ethanol vapor (Figure 10b). As the temperature increased, the resistance of the sensor decreased due to the generation of free carriers in the semiconductor, and a further decrease in temperature was accompanied by the recovery of the resistance almost to its initial value. Despite the increase in temperature, the resistance of the sensor hardly changes in the temperature range of 160–270 °C. It is assumed that in this temperature range the rate of free charge carriers generation in the semiconductor due to temperature rise is almost equal to the rate of adsorption of oxygen species on the active surface. It is revealed from Figure 10b that the response first increased with the temperature up to 250 °C and reduced in higher temperatures. The sensor showed an imperceptible response toward ethanol vapor at 50 °C and farther approached more than 117 at 250 °C. At a higher temperature (300 °C), a sharp decrease in response to the value of 22 was recorded. Therefore, the temperature of 250 °C was

selected as the optimum temperature to investigate the gas sensing characteristics of the ZnO<La> sensor. It is assumed that at temperatures smaller than 250 °C, the rate of ethanol adsorption and chemical reaction on the active surface is slowed down because at these temperatures the activation energies are not sufficient for kinetic processes to take place completely. At higher temperatures (>250 °C), the rate of desorption of gas molecules exceeds that of adsorption, which leads to a decrease in sensitivity. Gas sensing parameters of the ZnO<La> sensor at different operating temperatures in the presence of 675 ppm of ethanol vapor are summarized in Table 1.

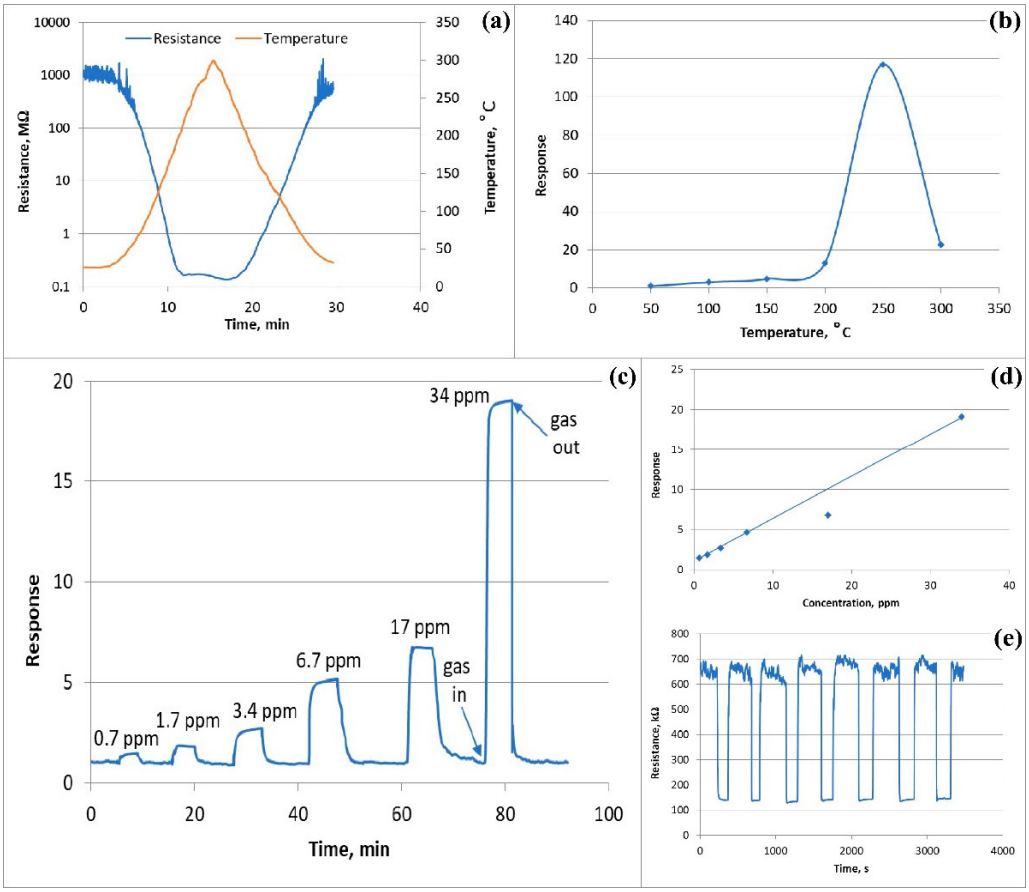

Figure 10. (**a**) Change in sensor resistance depending on the operating temperature in air, (**b**) response of the sensor to 675 ppm ethanol vapor in different temperatures, (**c**) dynamic response curves of the ZnO<La> sensor to different concentrations of ethanol at operating temperature, (**d**) ethanol concentration vs. sensor response, and (**e**) repeatability test of the sensor during seven cycles to 6.7 ppm ethanol.

Table 1. Gas sensing parameters of the ZnO<La> sensor at different temperatures in the presence of 675 ppm of ethanol vapor.

Temperature (°C)	Response Time (s)	Recovery Time (s)	Response
100	1.27×10^3	2.47×10^3	3.16
150	0.6×10^3	2.41×10^3	4.88
200	42	0.19×10^3	13.1
250	14	61	1.17×10^2
300	12	8	22.6

Metal oxide based sensors mainly operate in three temperature ranges. At higher temperatures (400–700 °C), kinetic processes on the semiconductor surface take place rapidly enough that equilibrium is immediately established between the bulk oxide and

the environment. Due to the reduced diffusion coefficient of oxygen species at medium temperatures (200–400 °C), the chemical composition of metal oxide does not reach equilibrium and the kinetic processes take place mainly on the semiconductor surface. For sensors operating in this temperature range, the use of thin films is preferable, as the main processes are performed mostly on the active surface. The ZnO<La> sensor with a thickness of 72 nm confirms this claim, as it works more efficiently at 250 °C. At lower operating temperatures (25–200 °C), the rate of ethanol adsorption and chemical reactions onto the sensor surface decrease, thus resulting to a reduction in sensor response.

The real-time responses of the ZnO<La> based sensor were measured at 250 °C operating temperatures toward different concentrations of ethanol vapor. Figure 10c shows the actual response-recovery curves of the sensor for ethanol vapor with concentrations varied from 0.7 to 34 ppm (at six different concentrations) at 250 °C. The typical response/recovery times were 14 and 60 s, respectively, confirming the fairly high speed of the sensor. A sensitivity was observed at extremely low concentrations of ethanol (0.7 ppm) and toward the higher concentration (34 ppm) the sensor response reached more than 19. The sensor response to the ethanol vapor increased linearly toward ethanol concentration varied from 0.7 to 34 ppm at 250 °C (Figure 10d). This will allow us to detect the ethanol vapor traces in real environments and accurately measure the low concentrations of this gas.

The repeatability of the sensor parameters is crucial for the long-term operation of the sensor, which is best characterized by a repeatability test of the response in real-time. Multiple measurements of the sensor response were performed toward 6.7 ppm ethanol vapor at 250 °C operating temperature to test the sensor drift over time. Figure 10e shows the repeatability test of the sensor performed for seven cycles of response and recovery curves, which represents almost the same response/recovery behavior and nearly matching response values confirming the fairly high repeatability.

The response and recovery times were estimated at different temperatures to compile the information on the sensor speed. The response and recovery times of the ZnO<La> sensor were calculated as the time is taken for rising and falling to 90% of the maximum response value after exposure to ethanol vapor and air, respectively. The response and recovery times decreased with the increase of the operating temperature approaching tens of seconds at higher temperatures (>200 °C) (Table 1). In the temperature range of 100 to 250 °C, the recovery time was definitely longer than the response time, while their values were quite close at higher temperatures (300 °C). It is assumed that the rate of gas desorption at the semiconductor surface exceeds the rate of adsorption at higher temperatures, which leads to a decrease both in the recovery time and in the sensor response. The dynamic resistance curve of the sensor showed that the response and recovery times of the sensor were found to be 14 and 61 s, respectively, for 675 ppm of ethanol vapors at an operating temperature of 250 °C (Figure 11a). The high speed of the sensor confirms its suitability for real-time detection of ethanol vapors.

To check the selectivity behavior in sensing performance, the ZnO<La> based sensor was examined in the presence of other interfering environmental gases. The sensor responses to 675 ppm ethanol, 785 ppm acetone, 3600 ppm water vapor, 650 ppm toluene, 700 ppm DMF, and 750 ppm ammonia were investigated at the 250 °C (Figure 11b). As it is evident, the sensor showed the highest response value to ethanol gas than other control gases. The dynamic response curves of the sensor for the above-mentioned gases confirm the high selectivity of the sensor towards ethanol vapor and the faster response/recovery behavior compared to that of the other gases (Figure 11c). Moreover, as a quantitative representation of the selectivity, the response ratios of ethanol to other gases ($S_{ethanol}/S_{other\ gases}$) were calculated, and the values were in the range of 7.7–49.7. It is noteworthy that the sensor showed an extremely low response toward humidity (S = 2.37 at 3600 ppm water vapor) allowing it to work in conditions of high relative environmental humidity.

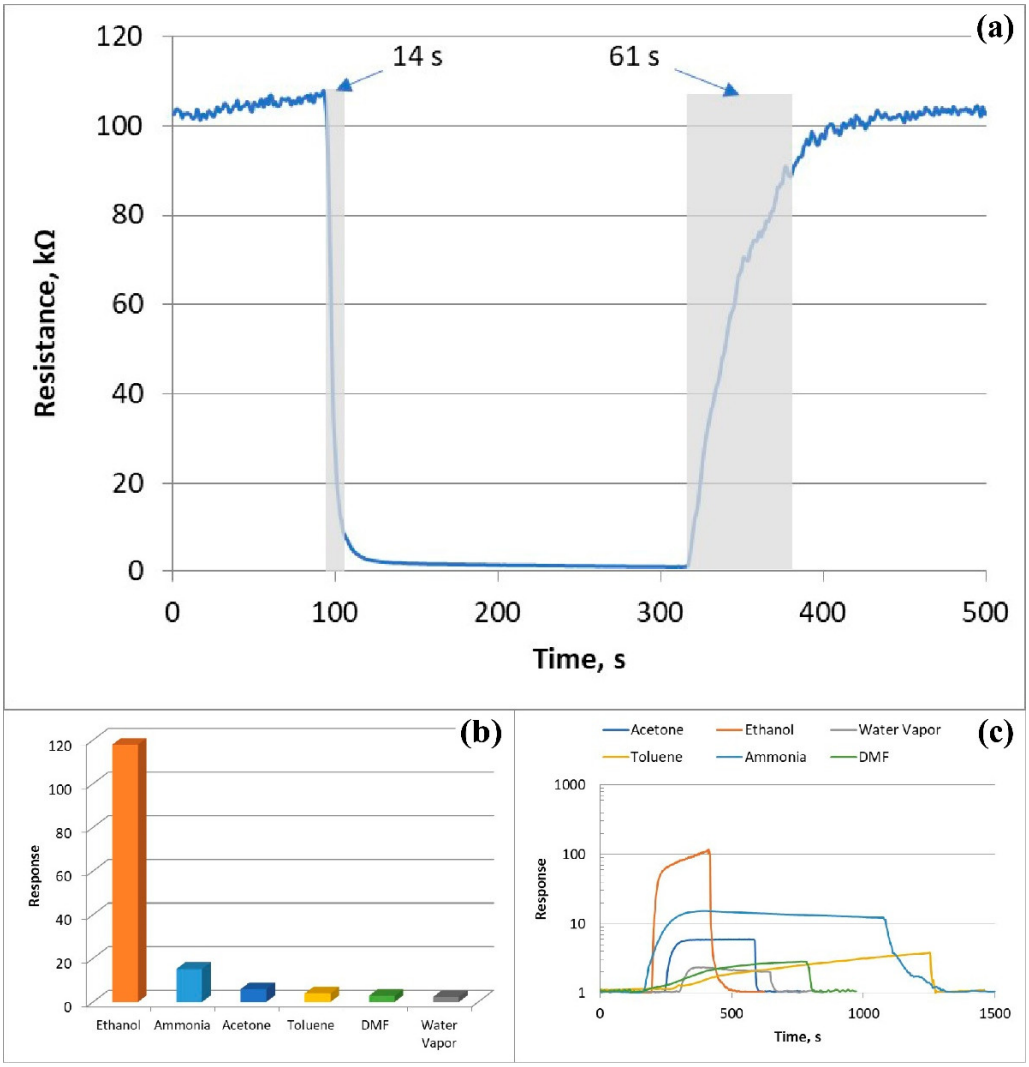

Figure 11. (**a**) Change in resistance of the sensor as a function of real-time reflecting the response and recovery time toward 675 ppm of ethanol, (**b**) selectivity of the sensor for ethanol at 250 °C, and (**c**) dynamic response curves of the sensor in the presence of different gases at 250 °C.

The sensing performance of the ZnO<La> sensor has been compared with reports related to ZnO-based C_2H_5OH sensors published in recent years. The corresponding results are summarized in Table 2 including the most important characteristics such as sensor material type, operating temperature, ethanol concentration, and response value. It is obvious from the comparison that the performance of the proposed ZnO<La> sensor is clearly comparable to that of other published reports. The most noticeable in the comparison is the extremely low detection limits of our sensor (0.7 ppm) at a relatively low operating temperature attributed to the discernible response value of 1.5.

Table 2. Performance comparison of the ethanol sensors based on ZnO materials.

Materials	T (°C)	Ethanol (ppm)	Response	Reference
Pd decorated ZnO nanorods	260	500	81%	[32]
Graphene/ZnO nanowires	125	20	26	[33]
CeO_2/ZnO nanosheets	310	100	90	[34]
ZnO<Ni> nanorods	150	100	376%	[35]

Table 2. *Cont.*

Materials	T (°C)	Ethanol (ppm)	Response	Reference
Ni-ZnO	370	500	313%	[36]
Co-ZnO plates	300	300	570%	[37]
ZnO<Bi> nanograin	400	1000	60%	[38]
ZnO<Mn> nanograins	240	20	11.4	[39]
ZnO<La>	250	675	117	This work
ZnO<La> nanograins	250	0.7	1.5	This work

It is noteworthy that the sensor based on pure ZnO material showed a poor sensitivity to ethanol vapors justifying the introduction of La into the main ZnO material. Besides, it is assumed that the introduction of La into ZnO material imports additional energy states in between the valence band and conduction band of zinc oxide reducing its bandgap energy. This reduces the sensor resistance by tuning it to a measurable range, while at the same time positively contributing to the gas sensing processes [30].

3.2. Gas Sensing Mechanism

The gas sensing mechanism for conductometric sensors based on semiconducting oxides works due to the adsorption and chemical reactions of target gas molecules on the active surface, as a result of which the sensor resistance changes. The chemisorbed oxygen species play a major role in the gas sensing mechanism. Thus, when the surface of the ZnO<La> layer contacts with air, oxygen molecules with sufficient activation energy adsorb on the sensor surface by trapping electrons from the conduction band of ZnO and form chemisorbed oxygen species (O^-(ads), O^{2-}(ads) and O_2^-(ads)), leading to the formation of the electron depletion layer. The supposed reactions can be described as follows [40–42]:

$$O_{2\,(gas)} \leftrightarrow O_{2\,(adsorbed)}, \quad (1)$$

$$O_{2\,(adsorbed)} + e^- \leftrightarrow O_2{}^-{}_{(adsorbed)}, \quad (2)$$

$$O_2{}^-{}_{(adsorbed)} + e^- \leftrightarrow 2O^-{}_{(adsorbed)}, \quad (3)$$

$$O^-{}_{(adsorbed)} + e^- \leftrightarrow O^{2-}{}_{(adsorbed)}, \quad (4)$$

The state of adsorbed oxygen species on the semiconductor surface is highly dependent on operating temperature. In a low temperature range (<200 °C), O^{2-} states predominate on the active surface, whereas in the range of 200 to 400 °C, the number of O^- states prevails. At higher operating temperatures (>400 °C), O^{2-} species begin to play a major role in the kinetic processes. For the ZnO<La> sensor, 250 °C was selected as the operating temperature, therefore the O^- species predominantly contributed to the sensing behavior. The oxygen chemisorption results in a modification of the space charge region toward depletion. The resistance corresponding to this state is considered the base resistance. For n-type semiconductors, the majority of charge carriers are electrons and upon interaction with a reducing gas, an increase in conductivity occurs. When the sensors are exposed to alcohol vapor, the ethanol molecules react with surface oxygen species and produce free electrons, resulting in an increase in electronic conductance. The supposed reactions can be described as follows [43–45]:

$$6O^-{}_{(adsorbed)} + C_2H_5OH_{\,(gas)} \rightarrow 3H_2O_{\,(gas)} + 2CO_{2\,(gas)} + 6e^-, \quad (5)$$

$$3O_2{}^-{}_{(adsorbed)} + C_2H_5OH_{\,(gas)} \rightarrow 3H_2O_{\,(gas)} + 2CO_{2\,(gas)} + 3e^-, \quad (6)$$

$$6O^{2-}{}_{(adsorbed)} + C_2H_5OH_{\,(gas)} \rightarrow 3H_2O_{\,(gas)} + 2CO_{2\,(gas)} + 12e^-. \quad (7)$$

Ethanol sensing mechanisms on the ZnO-based material were investigated by near-ambient-pressure X-ray photoelectron spectroscopy (NAP-XPS) [46], which showed the dehydrogenation of ethanol molecules, leading to ethoxy and acetaldehyde, where the detached hydrogens interact with the chemisorbed oxygen. These experimental results can be attributed to the support of the above-mentioned reactions.

If the sensing layer is fabricated from the metal oxide in nanoparticles form, the system is described by structural and band models of conductive mechanism. Without ethanol vapor, a high potential barrier (Schottky barrier) is formed between the adjacent nanograins leading to an increase in the film resistance. In the presence of ethanol molecules, as a result of the Reactions (5)–(7), the electrons are returned to the semiconductor lattice, which reduces the depletion region width, so the Schottky barriers are also lowered. A variation of the sensor resistance or electrical conductivity takes place as a result of the barrier height modulation [35]. The proposed schematic description of the C_2H_5OH sensing mechanism of the ZnO<La> material is shown in Figure 12.

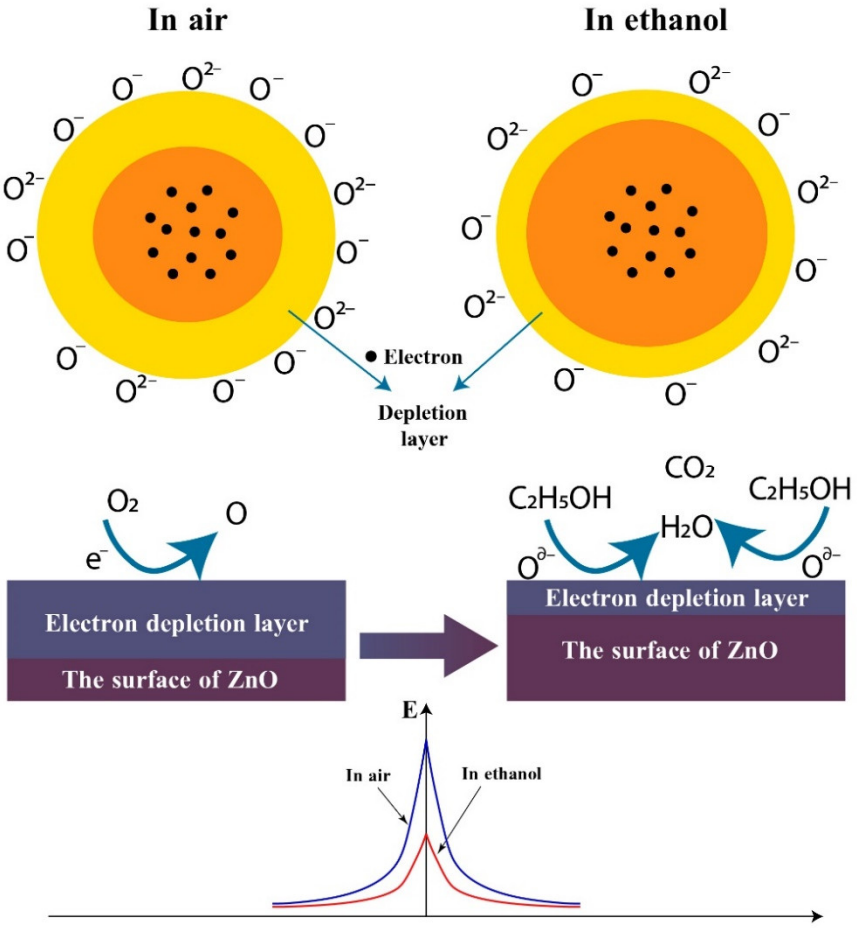

Figure 12. Schematic diagram of the proposed reaction mechanism of the ZnO to ethanol.

Pd compounds and Pd-based nanoparticles are mainly used as good catalysts for various gases [47]. Mainly, noble Pd nanoparticles form spillover zones around themselves on the semiconductor surface and promote O_2 dissociation leading to an increase in the number of chemisorbed oxygen species. The increased quantity of chemisorbed oxygen species and their reaction with the target gas molecules improve the sensing behavior. The sensitizing effect of palladium nanoparticles with the interaction of ethanol gas has been observed [32].

The high sensitivity for a metal oxide-based gas sensor is attributed to the grain size of the sensing film, which is comparable to, or smaller than, the twice Debye length ($d \leq 2L_D$), while the L_D is in the range of 20–22 nm for ZnO at 250–300 °C [48]. The grain sizes in

the ZnO<La> film are in the range of 20–40 nm, which definitely proves the high sensing behavior of our sensor.

4. Conclusions

In summary, the ZnO<La> sputtering target was prepared. A gas sensor based on the ZnO<La> thin film was fabricated by the RF magnetron sputtering method. The fabricated sensor device was investigated for ethanol sensing applications. The analysis of the EDX spectrum of the ZnO<La> material confirms the presence of Zn, La, and O peaks. The SEM images of the ZnO<La> based thin film (72 nm) prove its granular structure (nanoparticles with size: 20–40 nm) with a high homogeneity corresponding to 60 W of power generated and 20 s of deposition time. The elemental mapping analysis of the ZnO<La> film confirms that the elements Zn, Al, O, and La are uniformly distributed. Reasonable response values of 117 and 1.5 were measured at 250 °C toward 675 and 0.7 ppm ethanol concentration, respectively. The results indicated that the ZnO<La> based sensor has enhanced gas sensing properties, including a high response, superb selectivity, and a fast response/recovery time towards ethanol. The sensor also exhibits a dynamic transient response and repeatability for ethanol.

Author Contributions: This manuscript was written through the contributions of all authors. M.A. and V.A. were responsible for the management and coordination responsibility for the research activity planning and execution; M.A. also contributed to the fabrication of the gas sensors; A.S. and G.S. (Gevorg Shahkhatuni) were responsible for investigations of gas sensors including the measurements of gas sensing characteristics; Z.S. was responsible for designing all figures and providing study materials and references. G.S. (Gohar Shahnazaryan) contributed to the measurement of the thicknesses of the obtained metal oxide films and metal electrodes. All authors have read and agreed to the published version of the manuscript.

Funding: This research was funded by the Science Committee of RA, grant number № 21T-2J062.

Institutional Review Board Statement: Not applicable.

Informed Consent Statement: Not applicable.

Data Availability Statement: The data presented in this study are available on request to the corresponding author.

Acknowledgments: The authors would like to thank M. Zatikyan for the FTIR study of the ZnO<La> film.

Conflicts of Interest: The authors declare no conflict of interest.

References

1. Li, G.; Zhang, X.; Lu, H.; Yan, C.; Chen, K.; Lu, H.; Gao, J.; Yang, Z.; Zhu, G.; Wang, C.; et al. Ethanol sensing properties and reduced sensor resistance using porous Nb_2O_5-TiO_2 n-n junction nanofibers. *Sens. Actuators B Chem.* **2019**, *283*, 602–612. [CrossRef]
2. Boroujerdi, R.; Paul, R. Introducing Graphene–Indium Oxide Electrochemical Sensor for Detecting Ethanol in Aqueous Samples with CCD-RSM Optimization. *Chemosensors* **2022**, *10*, 42. [CrossRef]
3. Wang, C.; Li, R.; Feng, L.; Xu, J. The SnO_2/MXene Composite Ethanol Sensor Based on MEMS Platform. *Chemosensors* **2022**, *10*, 109. [CrossRef]
4. Ayyala, S.K.; Covington, J.A. Nickel-Oxide Based Thick-Film Gas Sensors for Volatile Organic Compound Detection. *Chemosensors* **2021**, *9*, 247. [CrossRef]
5. Wright, N.A.; Lee, L.-T. Alcohol-related traffic laws and drunk-driving fatal accidents. *Accid. Anal. Prev.* **2021**, *161*, 106358. [CrossRef]
6. Duko, B.; Pereira, G.; Betts, K.; Tait, R.J.; Newnham, J.; Alati, R. Associations of prenatal alcohol exposure and offspring harmful alcohol use: Findings from the Raine Study. *Drug Alcohol. Depend.* **2020**, *217*, 108305. [CrossRef]
7. Deng, X.; Zhang, L.; Guo, J.; Chen, Q.; Ma, J. ZnO enhanced NiO-based gas sensors towards ethanol. *Mater. Res. Bull.* **2017**, *90*, 170–174. [CrossRef]
8. Wahab, R.; Ahmad, N.; Alam, M.; Ahmad, J. Nanorods of ZnO: An effective hydrazine sensor and their chemical properties. *Vacuum* **2019**, *165*, 290–296. [CrossRef]
9. Wang, B.-R.; Wang, R.-Z.; Bai, Y.-J.; Liu, L.-Y.; Jiang, Q.-L. Zinc oxide nanonets with hierarchical crystalline nodes: High-performance ethanol sensors enhanced by grain boundaries. *J. Alloy. Compd.* **2021**, *877*, 160277. [CrossRef]

10. Tan, X.-Q.; Liu, J.-Y.; Niu, J.-R.; Liu, J.-Y.; Tian, J.-Y. Recent Progress in Magnetron Sputtering Technology Used on Fabrics. *Materials* **2018**, *11*, 1953. [CrossRef]
11. Xu, J.; Li, S.; Li, L.; Chen, L.; Zhu, Y. Facile fabrication and superior gas sensing properties of spongelike Co-doped ZnO microspheres for ethanol sensors. *Ceram. Int.* **2018**, *44*, 16773–16780. [CrossRef]
12. Juang, F.-R.; Chen, B.-Y. Effect of adding ZHS microcubes on ZnO nanorods for CO2 gas sensing applications. *Solid-State Electron.* **2020**, *164*, 107711. [CrossRef]
13. Aleksanyan, M.S.; Sayunts, A.G.; Shahkhatuni, G.H.; Aroutiounian, V.M.; Shahnazaryan, G.E. Study of Characteristics of the Sensor Detecting of Low Concentration of Ammonia. *J. Contemp. Phys. Armen. Acad. Sci.* **2021**, *56*, 352–358. [CrossRef]
14. Nie, C.; Zeng, W.; Li, Y. The 3D crystal morphologies of NiO gas sensor and constantly improved sensing properties to ethanol. *J. Mater. Sci. Mater. Electron.* **2018**, *30*, 1794–1802. [CrossRef]
15. Tharsika, T.; Thanihaichelvan, M.; Haseeb, A.S.M.A.; Akbar, S.A. Highly Sensitive and Selective Ethanol Sensor Based on ZnO Nanorod on SnO_2 Thin Film Fabricated by Spray Pyrolysis. *Front. Mater.* **2019**, *6*, 122. [CrossRef]
16. Zhang, K.; Lin, Z. Highly sensitive ethanol sensor based on zinc oxide-based nanomaterials with low power consumption. *J. Mater. Sci. Mater. Electron.* **2021**, *32*, 17395–17405. [CrossRef]
17. Subha, P.P.; Jayaraj, M.K. Enhanced room temperature gas sensing properties of low temperature solution processed ZnO/CuO heterojunction. *BMC Chem.* **2019**, *13*, 4. [CrossRef]
18. Ali, S.; Gupta, A.; Shafiei, M.; Langford, S.J. Recent Advances in Perylene Diimide-Based Active Materials in Electrical Mode Gas Sensing. *Chemosensors* **2021**, *9*, 30. [CrossRef]
19. Nasri, A.; Pétrissans, M.; Fierro, V.; Celzard, A. Gas sensing based on organic composite materials: Review of sensor types, progresses and challenges. *Mater. Sci. Semicond. Process.* **2021**, *128*, 105744. [CrossRef]
20. An, T.K.; Yun, H.-J.; Narote, R.; Kim, R.; Lee, S.U.; Kim, Y.; Nam, S.; Cha, H.; Jeong, Y.J.; Kim, K.; et al. Synthesis and characterization of an ester-terminated organic semiconductor for ethanol vapor detection. *Org. Electron.* **2014**, *15*, 2277–2284. [CrossRef]
21. Wei, H.-L.; Kumar, P.; Yao, D.-J. Printed Resistive Sensor Array Combined with a Flexible Substrate for Ethanol and Methane Detection. *ECS J. Solid State Sci. Technol.* **2020**, *9*, 115008. [CrossRef]
22. Aroutiounian, V.M.; Arakelyan, V.M.; Xachaturyan, E.A.; Shahnazaryan, G.E.; Aleksanyan, M.S.; Forro, L.; Magrez, A.; Her-nadi, K.; Nemeth, Z. Manufacturing and investigations of i-butane sensor made of SnO_2/multiwall-carbon-nanotube nanocomposite. *Sens. Actuators B Chem.* **2012**, *173*, 890–896. [CrossRef]
23. Pandeeswari, R.; Jeyaprakash, B.G. High sensing response of β-Ga2O3 thin film towards ammonia vapours: Influencing factors at room temperature. *Sens. Actuators B Chem.* **2014**, *195*, 206–214. [CrossRef]
24. Du, X.; George, S.M. Thickness dependence of sensor response for CO gas sensing by tin oxide films grown using atomic layer deposition. *Sens. Actuators B Chem.* **2008**, *135*, 152–160. [CrossRef]
25. Wilson, R.L.; Simion, C.E.; Blackman, C.S.; Carmalt, C.J.; Stanoiu, A.; Di Maggio, F.; Covington, J.A. The Effect of Film Thickness on the Gas Sensing Properties of Ultra-Thin TiO_2 Films Deposited by Atomic Layer Deposition. *Sensors* **2018**, *18*, 735. [CrossRef]
26. Kumar, M.; Kumar, A.; Gautam, Y.K.; Chandra, R.; Goyat, M.S.; Tewari, B.S.; Tewari, R.K. Influence of SiC thin films thickness on the electrical properties of Pd/SiC thin films for hydrogen gas sensor. *Vacuum* **2020**, *182*, 109750. [CrossRef]
27. Tian, J.; Jiang, H.; Deng, X.; Zhao, X.; Tian, J.; Shi, G.; Li, G.; Zhang, J.; Zhang, W. Response modulation of PdNi nano-film hydrogen sensors by thickness control. *Appl. Surf. Sci.* **2021**, *562*, 150064. [CrossRef]
28. Mauraya, A.K.; Singh, P.; Muthiah, S.; Kushvaha, S.S.; Muthusamy, S.K. Effect of post-oxidation processes and thickness of SnO2 films prepared by vacuum evaporation on CO gas sensing characteristics. *Ceram. Int.* **2021**, *47*, 13015–13022. [CrossRef]
29. Nandi, S.K.; Chakraborty, S.; Bera, M.K.; Maiti, C.K. Structural and optical properties of ZnO films grown on silicon and their applications in MOS devices in conjunction with ZrO2 as a gate dielectric. *Bull. Mater. Sci.* **2007**, *30*, 247–254. [CrossRef]
30. Manikandan, A.; Manikandan, E.; Meenatchi, B.; Vadivel, S.; Jaganathan, S.K.; Ladchumananandasivam, R.; Henini, M.; Maaza, M.; Aanand, J.S. Rare earth element (REE) lanthanum doped zinc oxide (La: ZnO) nanomaterials: Synthesis structural optical and antibacterial studies. *J. Alloys Compd.* **2017**, *723*, 1155–1161. [CrossRef]
31. Alamdari, S.; Ghamsari, M.S.; Lee, C.; Han, W.; Park, H.-H.; Tafreshi, M.J.; Afarideh, H.; Ara, M.H.M. Preparation and Characterization of Zinc Oxide Nanoparticles Using Leaf Extract of Sambucus ebulus. *Appl. Sci.* **2020**, *10*, 3620. [CrossRef]
32. Cao, P.; Yang, Z.; Navale, S.T.; Han, S.; Liu, X.; Liu, W.; Lu, Y.; Stadler, F.J.; Zhu, D. Ethanol sensing behavior of Pd-nanoparticles decorated ZnO-nanorod based chemiresistive gas sensors. *Sens. Actuators B Chem.* **2019**, *298*, 126850. [CrossRef]
33. Rafiee, Z.; Roshan, H.; Sheikhi, M.H. Low concentration ethanol sensor based on graphene/ZnO nanowires. *Ceram. Int.* **2021**, *47*, 5311–5317. [CrossRef]
34. Hui, G.; Zhu, M.; Yang, X.; Liu, L.; Pan, G.; Wang, Z. Highly sensitive ethanol gas sensor based on CeO2/ZnO binary heterojunction composite. *Mater. Lett.* **2020**, *278*, 128453. [CrossRef]
35. Sudha, M.; Radha, S.; Kirubaveni, S.; Kiruthika, R.; Govindaraj, R.; Santhosh, N. Experimental study on structural, optoelectronic and room temperature sensing performance of Nickel doped ZnO based ethanol sensors. *Solid State Sci.* **2018**, *78*, 30–39. [CrossRef]
36. Xu, M.; Li, Q.; Ma, Y.; Fan, H. Ni-doped ZnO nanorods gas sensor: Enhanced gas-sensing properties, AC and DC electrical behaviors. *Sens. Actuators B Chem.* **2014**, *199*, 403–409. [CrossRef]
37. Darvishnejad, M.H.; Firooz, A.A.; Beheshtian, J.; Khodadadi, A.A. Highly sensitive and selective ethanol and acetone gas sensors by adding some dopants (Mn, Fe, Co, Ni) onto hexagonal ZnO plates. *RSC Adv.* **2016**, *6*, 7838–7845. [CrossRef]

38. Zahirullah, S.S.; Immanuel, P.; Pravinraj, S.; Inbaraj, P.F.H.; Prince, J.J. Synthesis and characterization of Bi doped ZnO thin films using SILAR method for ethanol sensor. *Mater. Lett.* **2018**, *230*, 1–4. [CrossRef]
39. Wang, J.; Yang, J.; Han, N.; Zhou, X.; Gong, S.; Yang, L.; Hu, P.; Chen, Y. Highly sensitive and selective ethanol and acetone gas sensors based on modified ZnO nanomaterials. *Mater. Des.* **2017**, *121*, 69–76. [CrossRef]
40. Vijayalakshmi, K.; Jereil, S.D. Enhanced ethanol sensing performance of Fe: TiO_2 nanowires and their mechanism of sensing at room temperature. *Ceram. Int.* **2015**, *41*, 3220–3226. [CrossRef]
41. Afrouzmehr, M.; Yasrebi, N.; Sheikhi, M.H. Fabrication and characterization of Ag-Decorated indium–tin-oxide nanoparticle based ethanol sensors using an enhanced electrophoretic method. *Ceram. Int.* **2021**, *47*, 30504–30513. [CrossRef]
42. Cheng, Y.; Guo, H.; Wang, Y.; Zhao, Y.; Li, Y.; Liu, L.; Li, H.; Duan, H. Low cost fabrication of highly sensitive ethanol sensor based on Pd-doped α-Fe 2 O 3 porous nanotubes. *Mater. Res. Bull.* **2018**, *105*, 21–27. [CrossRef]
43. Umar, A.; Ibrahim, A.A.; Nakate, U.T.; Albergi, H.; Alsaiari, M.A.; Ahmed, F.; Alharthi, F.A.; Alghamdi, A.A.; Al-Zaqri, N. Fabrication and characterization of CuO nanoplates based sensor device for ethanol gas sensing application. *Chem. Phys. Lett.* **2021**, *763*, 138204. [CrossRef]
44. Wang, L.; Ma, S.; Xu, X.; Li, L.; Yang, T.; Cao, P.; Yun, P.; Wang, S.; Han, T. Oxygen vacancy-based Tb-doped SnO2 nanotubes as an ultra-sensitive sensor for ethanol detection. *Sens. Actuators B Chem.* **2021**, *344*, 130111. [CrossRef]
45. Liu, H.; Fan, H.-T.; Xu, X.-J.; Lu, H.; Zhang, T. Synthesis and gas sensing characteristics of LaxSr1−xFeO3 nanofibers via electrospinning. *Solid-State Electron.* **2013**, *79*, 87–91. [CrossRef]
46. Piliai, L.; Tomeček, D.; Hruška, M.; Khalakhan, I.; Nováková, J.; Fitl, P.; Yatskiv, R.; Grym, J.; Vorokhta, M.; Matolínová, I.; et al. New Insights towards High-Temperature Ethanol-Sensing Mechanism of ZnO-Based Chemiresistors. *Sensors* **2020**, *20*, 5602. [CrossRef] [PubMed]
47. Tsuji, J. *Palladium Reagents and Catalysts: New Perspectives for the 21st Century*, 1st ed.; John Wiley & Sons Ltd.: Chichester, UK, 2004; pp. 1–26.
48. Ren, Q.; Cao, Y.-Q.; Arulraj, D.; Liu, C.; Wu, D.; Li, W.-M.; Li, A.-D. Review—Resistive-Type Hydrogen Sensors Based on Zinc Oxide Nanostructures. *J. Electrochem. Soc.* **2020**, *167*, 067528. [CrossRef]